American Mineralogist, Volume 74, pages 203–215, 1989

Characterization of clay minerals by ^{27}Al nuclear magnetic resonance spectroscopy

DONALD E. WOESSNER
Mobil Research and Development Corporation, Dallas Research Laboratory, 13777 Midway Road, Dallas, Texas 75244, U.S.A.

ABSTRACT

^{27}Al isotropic chemical shifts and the nuclear electric quadrupole coupling parameter (a function of both the quadrupole coupling constant and the asymmetry parameter) have been determined for a wide variety of 2:1 clay minerals using magic-angle-spinning nuclear magnetic resonance spectroscopy at H_0 magnetic fields of 6.35 and 11.74 T, proton decoupling, and high-speed sample spinning (8.9 kHz at 6.35 T and 5.3 kHz at 11.74 T). The $^{[4]}Al$ chemical shifts become progressively deshielded (more positive) with increasing $^{[4]}Al$ for Si substitution and increasing total layer charge, in the same manner as found by previous authors for ^{29}Si. The $^{[4]}Al$ nuclear electric quadrupole coupling parameter also increases with increasing $^{[4]}Al$ substitution and total layer charge. Both quantities are related to tetrahedral layer distortion. The $^{[4]}Al$ chemical shift is more shielded for trioctahedral (Mg) phases than dioctahedral (Al) phases, as noted previously for ^{29}Si. The $^{[6]}Al$ MAS NMR peaks of gibbsite, beidellite, and other minerals show multiple Al electrostatic site environments. This peak is broader for dioctahedral phases containing Mg. $^{[4]}Al/^{[6]}Al$ quantitation using the 11.74-T spectra is in excellent agreement with published structural formulae. The high spinning speed contributes significantly to this agreement. The amount of $^{[4]}Al$ in montmorillonites is either small or undetectable, and the published structural formulae for some of them apparently do not represent the actual composition of the clay used in this study. High-field, high-speed spinning ^{27}Al MAS NMR measurement is a direct and sensitive technique for distinguishing montmorillonite from beidellite.

INTRODUCTION

Since 1979 there has been a growing use of high-resolution magic-angle spinning (MAS) nuclear magnetic resonance (NMR) spectroscopy to study minerals (Kirkpatrick et al., 1985b; Oldfield and Kirkpatrick, 1985). The early work concentrated on ^{29}Si, because ^{29}Si MAS NMR spectra have narrow, well-resolved peaks and, thus, much structural information. Measurements on quadrupolar nuclei such as ^{27}Al were initially avoided, because the nuclear electric quadrupole interaction produces very broad NMR peaks for powder samples. However, in 1982 it was shown that relatively high resolution spectra can be obtained under conditions of magic-angle spinning, very high magnetic field strengths (H_0) and observation of solely the ($\frac{1}{2}$, $-\frac{1}{2}$) spin transition (Meadows et al., 1982).

This paper explores the relationships of the ^{27}Al NMR chemical shifts and of nuclear electric quadrupole coupling parameters (Hafner and Hartmann, 1964; Ghose and Tsang, 1973; Villa and Bjorkstam, 1983; Shulepov et al., 1983; Kirkpatrick et al., 1985a) to the atomic substitutions in the tetrahedral and octahedral sheets of 2:1 clay minerals. This work differs from most earlier ^{27}Al MAS NMR work on clays (Alma et al., 1984; Barron et al., 1985; Diddams et al., 1984; Goodman and Stucki, 1984; Kinsey et al., 1985; Kirkpatrick et al., 1985b; Komareni et al., 1986; Lippmaa et al., 1986; Lipsicas et al., 1984; Plee et al., 1985; Sanz and Serratosa, 1984a, 1984b; Thompson, 1984) in several important aspects. (1) Many different types of 2:1 clay minerals were studied to allow comprehensive comparison of the ^{27}Al MAS NMR characteristics to clay structural and compositional parameters. (2) The sample spinning speeds were higher, greatly increasing the clarity of the spectra by reducing the number and intensity of interfering spinning sidebands. The spinning speeds were chosen to remove the spinning sidebands of the $^{[6]}Al$ peak from the spectral region containing the peak for $^{[4]}Al$. (3) Proton decoupling was used routinely, significantly increasing the resolution. (4) Most samples were measured at two magnetic fields.

It is important to obtain data at several H_0 field strengths because the first moment (the center of gravity), M1, of the ($\frac{1}{2}$, $-\frac{1}{2}$) MAS NMR peak of a quadrupolar nucleus in a powder sample differs from the isotropic chemical shift (Behrens and Schnabel, 1982). This second-order quadrupole shift and the width of the observed NMR peak decrease with increasing H_0 magnetic field (Behrens and Schnabel, 1982; Ganapathy et al., 1982). The isotropic chemical shift, δ_i, and the second-order quadrupole effect parameter (SOQE = (QCC) $(1 + \eta^2/3)^{1/2}$, where QCC is the quadrupole coupling constant and η is the asymmetry parameter) can be determined from the M1 values measured at two different H_0 strengths (Lippmaa et al., 1986). When multiple sites contribute to the NMR peaks, the δ_i obtained in this fashion is the weighted average isotropic

0003–004X/89/0102–0203$02.00

TABLE 1. Names, localities, and structural formulae for 2:1 silicates examined in this study

Name (ref.)*	Locality	Structural formula†
Beidellite (1)	Black Jack mine, Idaho	$M^{+}_{1.10}[(Al_{3.91}Mg_{0.02}Fe_{0.06})(Si_{6.95}Al_{1.05})O_{20}(OH)_4]$
Saponite (1)	Ballarat, California	$M^{+}_{0.98}[(Mg_{5.79}Al_{0.12}Fe_{0.07})(Si_{6.85}Al_{1.15})O_{20}(OH)_4]$
Saponite (2)	Allt Ribhein, Skye, Scotland	$M^{+}_{1.02}[(Mg_{5.84}Al_{0.03}Mn_{0.01}Fe^{3+}_{0.08})(Si_{6.99}Al_{1.01})O_{20}(OH_4)]$
Synthetic saponite	Tem-Press Research, Inc.	N.A.
Montmorillonite (3)	Tatatilla, Vera Cruz, Mexico	$M^{+}_{1.04}[(Al_{3.15}Mg_{0.85}Fe^{3+}_{0.01})(Si_{7.80}Al_{0.20})O_{20}(OH)_4]$
Montmorillonite (4)	Crook County, Wyoming	$M^{+}_{0.88}[(Al_{2.94}Mg_{0.64}Fe^{3+}_{0.36}Fe^{2+}_{0.04})(Si_{7.88}Al_{0.12})O_{20}(OH)_4]$
Montmorillonite (3)	Apache County, Arizona	$M^{+}_{0.97}[(Al_{2.95}Mg_{0.76}Fe^{3+}_{0.25}Fe^{2+}_{0.04})(Si_{7.79}Al_{0.21})O_{20}(OH)_4]$
Montmorillonite (3)	Clay Spur, Wyoming	$M^{+}_{0.85}[(Al_{3.06}Mg_{0.52}Fe^{3+}_{0.42})(Si_{7.68}Al_{0.32})O_{20}(OH)_4]$
Montmorillonite (3)	Belle Fourche, South Dakota	$M^{+}_{0.70}[(Al_{3.11}Mg_{0.57}Fe^{3+}_{0.34}Fe^{2+}_{0.02})(Si_{7.80}Al_{0.20})O_{20}(OH)_4]$
Montmorillonite (3)	Polkville, Mississippi	$M^{+}_{0.91}[(Al_{2.89}Mg_{0.94}Fe^{3+}_{0.17})(Si_{8.00})O_{20}(OH)_4]$
Montmorillonite (5)	Umiat, Alaska	$M^{+}_{0.84}[(Al_{2.96}Mg_{0.64}Fe^{3+}_{0.36})(Si_{7.84}Al_{0.16})O_{20}(OH)_4]$
Montmorillonite (3)	Otay, California	$M^{+}_{1.18}[(Al_{2.69}Mg_{1.20}Fe^{3+}_{0.11})(Si_{7.95}Al_{0.05})O_{20}(OH)_4]$
Montmorillonite (6)	Almeria, Spain	$M^{+}_{1.42}[(Al_{3.24}Mg_{0.77}Fe^{3+}_{0.19}Mn_{0.01})(Si_{7.34}Al_{0.66})O_{20}(OH)_4]$
Illite (7)	Interlake well, Montana	$M^{+}_{1.86}[(Al_{3.24}Mg_{0.60}Fe^{3+}_{0.06}Fe^{2+}_{0.10})(Si_{6.80}Al_{1.20})O_{20}(OH)_4]$
Illite (8)	Wind River Canyon, Wyoming	$M^{+}_{1.60}[Al_{3.32}Mg_{0.60}Fe^{3+}_{0.06}Fe^{2+}_{0.10})(Si_{6.86}Al_{1.14})O_{20}(OH)_4]$
Synthetic (9) mica-montmorillonite	Baroid Div., NL Industries	$M^{+}_{1.26}[(Al_4)(Si_{6.58}Al_{1.42})O_{20}(OH,F)_4]$
Rectorite (10)	Garland County, Arkansas	$M^{+}_{1.89}[(Al_{3.971})(Si_{6.603}Al_{1.397})O_{22}(OH)_4]$
Ordered Illite/Smectite	Zemplini, Hungary	N.A.
Mg chlorite	Carbago, New South Wales, Australia	N.A.
Cookeite (11)	North Little Rock, Arkansas	$(LiAl_4)(Si_3Al)O_{10}(OH)_8$
Vermiculite (12)	Llano, Texas	$M^{+}_{1.97}[(Mg_{5.66}Al_{0.30}Fe_{0.02})(Si_{5.72}Al_{2.28})O_{20}(OH)_4]$
Ephesite (13)	Hotazel, Cape Providence, South Africa	$Na^{+}[(LiAl_2)(Si_2Al_2)O_{10}(OH)_2]$
Palygorskite (14)	Gadsden County, Florida	$Ca^{2+}_{0.32}[(Al_{1.29}Mg_{1.96}Fe^{3+}_{0.37}Fe^{2+}_{0.03})(Si_{7.79}Al_{0.21})O_{20}(OH)_2(OH_2)_4\cdot 4H_2O]$
Pyrophyllite (11)	Moore County, North Carolina	$Al_4Si_8O_{20}(OH)_4$
Synthetic gibbsite (11)	Alcoa Aluminum	$Al(OH)_3$

Note: N.A. = not available.

* Reference for chemical analysis: (1) Callaway and McAtee (1985); (2) Mackenzie (1957); (3) Schultz (1969); (4) Van Olphen and Fripiat (1979); (5) Anderson and Reynolds (1966); (6) Mackenzie (1960); (7) Hower and Mowatt (1966); (8) Kinsey et al. (1985); (9) Komareni et al. (1986); (10) Barron et al. (1985); (11) assumed stoichiometric composition; (12) Shirozu and Bailey (1966); (13) Schaller et al. (1967); (14) Bradley (1940).

† Sources of chemical analyses are from references noted in column one.

chemical shift and the SOQE is the root-mean-square weighted-average value.

Experimental methods

Samples

The samples examined, their structural formulae, and sources are listed in Table 1. All of the samples were characterized by X-ray powder diffraction. The presence of impurity phases that could affect the ^{27}Al NMR spectra is indicated in the text.

NMR spectrometers

Measurements at 6.35 T were made using a JEOL FX-270 NMR spectrometer and a Chemagnetics 8.9-kHz sample spinner with Torlon rotors of 0.10-cm^3 sample volume. The radio-frequency pulses were 5.7-μs 90° pulses (⅓ of a solution 90° pulse). Spectra obtained with this instrument contain a weak $^{[6]}$Al peak near 0 ppm due to a small quantity of Al-containing impurities in the Torlon. The measured NMR waveforms were transferred to a Nicolet 1180 NMR computer for data analysis. For calculating M1 of a complex NMR spectral band, this computer has a routine that is not included in the JEOL FX NMR software.

Measurements at 11.74 T were made using a Bruker AM-500 NMR spectrometer and a typical sample-spinning speed of 5.3 kHz with Delrin rotors of 0.20-cm^3 sample volume. The radio frequency pulses were 1.0-μs 30° pulses (⅑ of a solution 90° pulse). The Bruker NMR software does not provide for evaluation of M1 values, and only the peak chemical-shift values at the maximum intensity, δ_p, were determined.

Measurements on several samples at 2.35 T were made using a JEOL FX-60 NMR spectrometer console in conjunction with a Chemagnetic 2.35-T solids accessory with a spinning speed of 3.5 kHz and Delrin rotors of 0.51-cm^3 sample volume. The radio-frequency pulses were 2.0-μs 45° pulses (⅛ of a solution 90° pulse). The measured NMR waveforms were transferred to a MicroVax II computer for data analysis. This computer has a software routine for calculating M1.

Calculations

The 6.35-T peaks were integrated with the Nicolet 1180 software. Some of the 11.74-T peaks were integrated with the Bruker software, but most were integrated by cutting out the peaks and weighing the paper.

We used the method of Lippmaa et al. (1986) and the 6.35-T M1 values and the 11.74-T peak maximum position δ_p (Table 2) to calculate the $^{[4]}$Al isotropic chemical shift δ_i and the second-order quadrupole effect parameter. Because M1 was not determined at 11.74 T, the observed δ_p was used for this calculation. This is a good approximation, because the 11.74 T $^{[4]}$Al peaks are nearly symmetric and the second-order quadrupole shift is small at this H_0 field strength. If measured M1 values were used, the δ_i and SOQE values would be smaller. The estimated maximum errors are 0.5 ppm and 0.1 MHz, respectively.

The methods of Ganapathy et al. (1982) were used to calculate theoretical peaks (e.g., Figs. 1 and 2).

Results

Model compounds

The measured and calculated ^{27}Al MAS NMR spectra of the model materials gibbsite (Fig. 3), pyrophyllite (Fig.

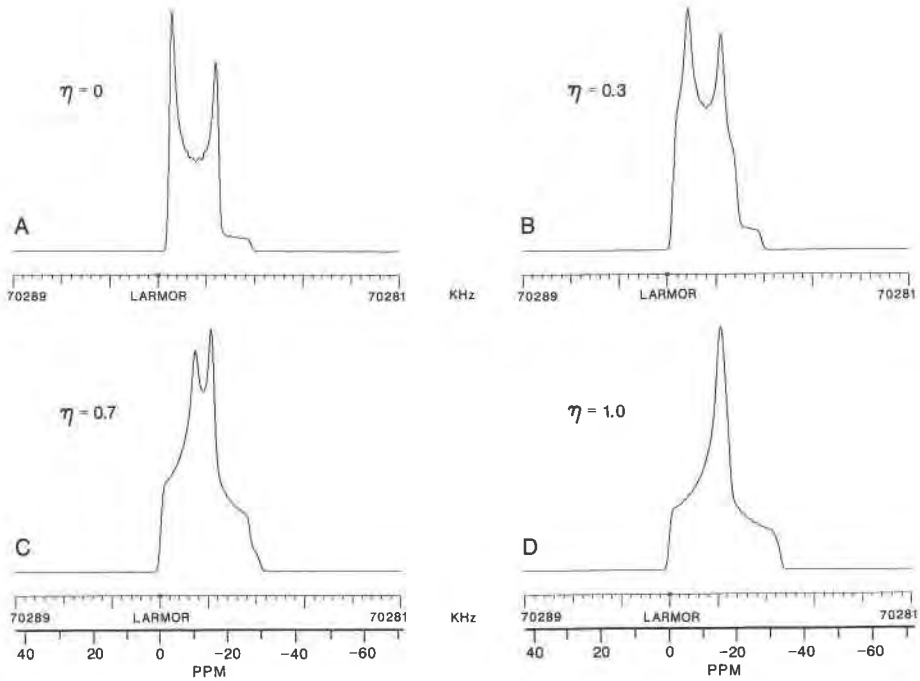

Fig. 1. Simulated 6.35-T ^{27}Al MAS NMR spectra at four different values of η for QCC = 3.0 MHz with 100-Hz Gaussian line broadening.

4), and beidellite (Fig. 5) provide a framework for the interpretation of the spectra of the clays. These spectra enable us to determine some consequences of site substitution on NMR peak shapes and positions.

Clay minerals

Figures 6 and 7 present 6.35-T and 11.74-T spectra, respectively, of a variety of clay minerals. The spinning sidebands are indicated by an asterisk and impurity peaks

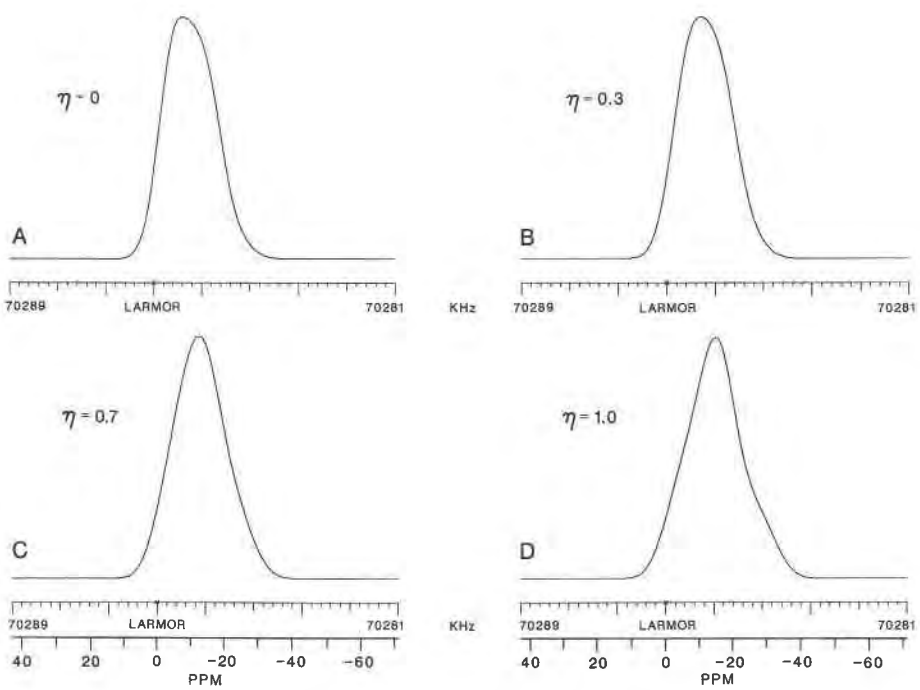

Fig. 2. Simulated 6.35-T ^{27}Al MAS NMR spectra at four different values of η for QCC = 3.0 MHz with 700-Hz Gaussian line broadening.

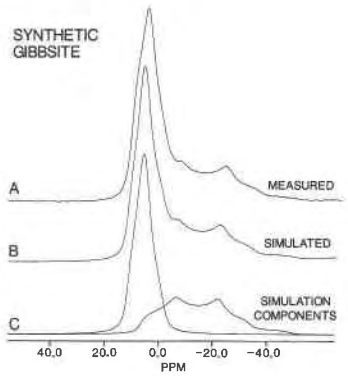

Fig. 3. Measured (**A**) and simulated (**B**) 6.35-T ^{27}Al MAS NMR spectra of synthetic gibbsite, together with the simulation components (**C**).

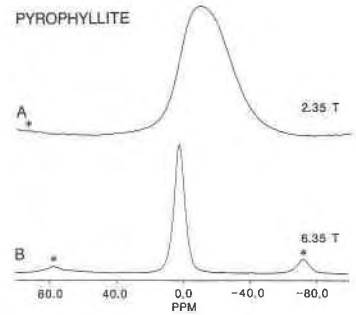

Fig. 4. ^{27}Al MAS NMR spectra of pyrophyllite at 2.35 T and 6.35 T. The asterisk signifies spinning sidebands.

by an I. At 6.35 T, the high spinning speeds eliminate spinning sidebands between the $^{[4]}$Al and $^{[6]}$Al peaks, which for some samples are broad enough to observe structural information. At 11.74 T, there is an $^{[6]}$Al spinning sideband together with an occasional overlapping $^{[4]}$Al spinning sideband between the $^{[4]}$Al and $^{[6]}$Al peaks (Fig. 7). Compared to the 6.35-T spectra, these peaks are much narrower, because the second-order quadrupolar broadening (in ppm units) is 3.44 times smaller (Behrens and Schnabel, 1982).

The observed peak maxima, δ_p, at both H_0 field strengths and the 6.35-T M1 values are listed in Table 2. The M1 values for the $^{[6]}$Al may have some error, because, even at the 8.9-kHz spinning speed, the large linewidths cause spinning-sideband artifacts that distort the peak. The MAS NMR linewidths at 6.35 T are several times broader than at 11.74 T (Table 3). The $^{[4]}$Al/($^{[4]}$Al + $^{[6]}$Al) ratios obtained by integrating the center peaks for $^{[4]}$Al and $^{[6]}$Al agree remarkably well in most cases with the values calculated from the structural formula (Table 4). Some of the $^{[4]}$Al/($^{[4]}$Al + $^{[6]}$Al) ratios obtained from the 6.35-T spectra are significantly greater than the 11.74-T values. In these cases, in the 6.35-T spectra, the tail of the first spinning sideband of the broad octahedral peak contributes to the area under the tetrahedral peak, even at 8.9-kHz spinning speed.

The δ_i and SOQE values calculated with the method of Lippmaa et al. (1986) are shown in Table 5.

Pyrophyllite and palygorskite have small $^{[6]}$Al QCC values; therefore we made measurements at a lower H_0 strength (2.35 T).

The present results show an asymmetry (i.e., $\delta_p >$ M1) in many $^{[6]}$Al peak shapes that has not been previously discussed but is apparent in some published spectra (Diddams et al. 1984; Lipsicas et al., 1984; Barron et al., 1985; Komareni et al., 1986). The higher spinning speeds utilized here move the first spinning sidebands farther away from the center peak and decrease their amplitudes, allowing improved definition of the center-peak shape.

TABLE 2. ^{27}Al MAS NMR peak positions (δ_p) at 6.35 T and 11.74 T and the M1 values at 6.35 T

	Tetrahedral Al			Octahedral Al		
Mineral	δ_p (6.35 T) (ppm)	M1 (ppm)	δ_p (11.74 T) (ppm)	δ_p (6.35 T) (ppm)	M1 (ppm)	δ_p (11.74 T) (ppm)
Black Jack beidellite	64.8	64.4	70.0	3.1	−7.1	4.1
Ballarat saponite	62.7	60.0	65.7	—	—	—
Allt Ribhein saponite	60.4	56.4	65.2	—	—	—
Synthetic saponite	62.7	58.4	65.6	7.9	−3.4	9.5
Tatatilla montmorillonite	66.3	63.9	68.8	3.2	−1.9	3.2
Wyoming montmorillonite	—	—	—	−0.7	−16.7	3.2
Arizona montmorillonite	—	—	—	2.0	−17.7	2.7
Interlake illite	65.7	61.6	69.3	2.9	−11.6	3.5
Wind River illite	65.4	61.9	69.0	2.9	−5.5	3.2
Synthetic mica-montmorillonite	66.5	63.1	69.7	2.9	−3.4	3.7
Rectorite	69.9	67.3	71.8	3.5	−3.4	4.6
Zemplini I/S	66.3	62.5	69.9	3.5	−4.9	4.2
Carbago chlorite	66.5	57.7	68.8	7.0	4.5	8.9
Cookeite	66.8	62.8	71.0	3.7	2.1	5.7
Vermiculite	63.8	53.5	66.6	—	—	8.3
Ephesite	68.5	67.1	74.0	−11.8	−31.1	2.4
				−47.1	—	−12.6
Palygorskite	—	—	57.0	3.5	4.5	3.9
Pyrophyllite	—	—	—	2.4	2.4	3.8

Note: The chemical shifts and M1 values measured with respect to 1 molar $Al(H_2O)_6Cl_3$ in H_2O as external reference.

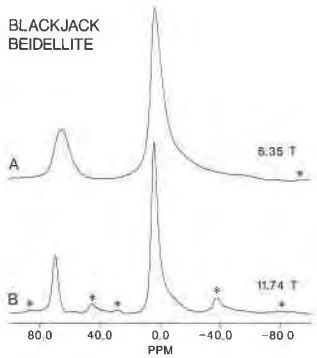

Fig. 5. ^{27}Al MAS NMR spectra of Black Jack beidellite at 6.35 T and 11.74 T. The asterisk signifies spinning sidebands.

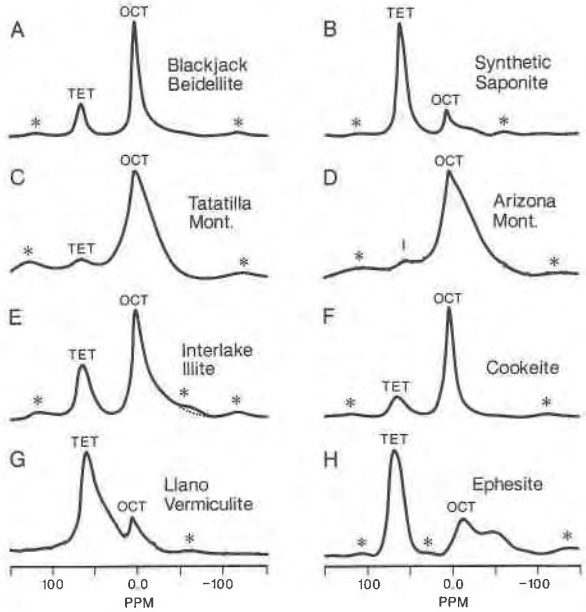

Fig. 6. ^{27}Al MAS NMR spectra of layer silicates at 6.35 T. The asterisk signifies spinning sidebands and I signifies impurities.

Discussion

Correlations with $^{[4]}$Al/(Si + $^{[4]}$Al) and total layer charge

Previous work (Weiss et al., 1987) has shown that ^{29}Si δ_i values for sheet silicates correlate well with total layer charge and parameters related to the distortion of the tetrahedral sheet. The results presented here show that $^{[4]}$Al SOQE and δ_i also correlate well with these parameters.

For minerals with the same type of octahedral sheet, $^{[4]}$Al-for-Si substitution is the main cause of distortion in the tetrahedral sheet and, as for ^{29}Si chemical shifts (Weiss et al., 1987), $^{[4]}$Al/($^{[4]}$Al + Si) correlates well with progressively deshielded $^{[4]}$Al chemical shifts (Fig. 8). These results agree well with the same conclusion drawn by Kinsey et al. (1985). The data of Lippmaa et al. (1986) for margarite and muscovite are included in this analysis. Some data points are not used in the least-squares fits (Table 6), because they represent special cases (see Discussion of Individual Phases). In Figure 8, the data for the dioctahedral layer phases (montmorillonite, cookeite, and margarite) and ephesite (trioctahedral, $LiAl_2$) fall along the upper line. The data for muscovite (open square) does

Table 3. ^{27}Al MAS NMR linewidths at 6.35 T and 11.74 T

Mineral	Tetrahedral Al		Octahedral Al		Ratio of LW at 7.35 T to LW at 11.74 T	
	LW (6.35 T) (ppm)	LW (11.74 T) (ppm)	LW (6.35 T) (ppm)	LW (11.74 T) (ppm)	Octahedral	Tetrahedral
Black Jack beidellite	11.9	4.2	8.9	4.4	2.0	2.8
Ballarat saponite	12.5	4.2	—	—	—	2.7
Allt Ribhein saponite	20.5	5.0	—	—	—	4.1
Synthetic saponite	13.1	5.2	10.8	3.3	3.3	2.5
Tatatilla montmorillonite	19.0	5.5	33.1	10.2	3.2	3.5
Wyoming montmorillonite	—	—	42.2	12.6	3.3	—
Arizona montmorillonite	—	—	40.8	13.0	3.1	—
Arizona montmorillonite (purified)				12.0		
Clay Spur montmorillonite				12.1		
Belle Fourche montmorillonite				13.6		
Polkville montmorillonite				12.5		
Umiat montmorillonite				10.7		
Otay montmorillonite				8.5		
Almeria montmorillonite				8.6		
Interlake illite	19.7	7.4	16.9	9.0	1.9	2.7
Wind River illite	25.0	7.6	21.9	8.9	2.5	3.3
Synthetic mica-montmorillonite	21.1	7.3	20.0	7.8	2.6	2.9
Rectorite	15.3	5.1	14.2	5.1	3.0	2.8
Zemplini I/S	24.2	6.3	22.5	6.8	3.3	3.8
Carbago chlorite	—	—	9.2	4.3	2.1	—
Cookeite	22.2	7.5	11.7	6.3	1.9	3.0
Vermiculite	30.6	10.1	—	—	—	3.0
Ephesite	19.9	5.8	58.6	17.5	3.3	3.4
Palygorskite	—	—	6.8	3.0	2.3	—

Note: The linewidths, LW, are the full linewidths at half height. These values have had removed from them the nominal line broadening (typically 0.5 ppm) employed in processing the measured waveforms.

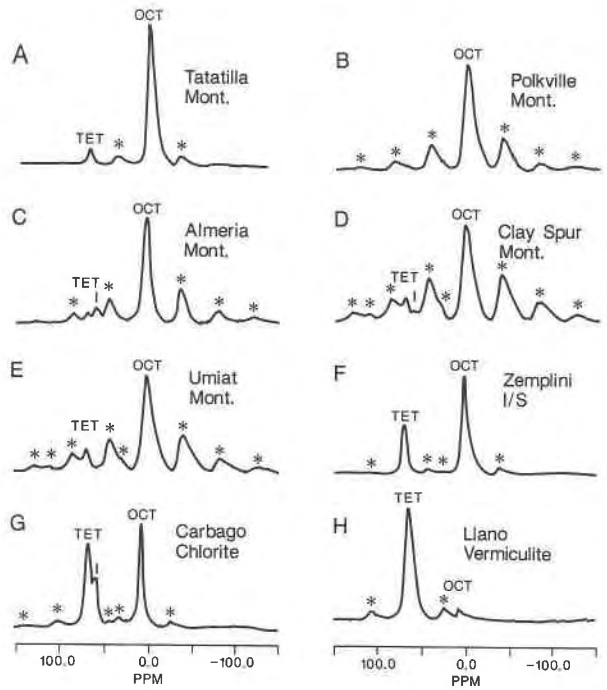

Fig. 7. ^{27}Al MAS NMR spectra of layer silicates at 11.74 T. The asterisk signifies spinning sidebands and I signifies impurities.

not fall along this line. The data for the Mg-substituted trioctahedral phases (saponite and vermiculite) fall along the lower line, in agreement with the trend observed for ^{29}Si (Weiss et al., 1987).

The $^{[4]}$Al chemical shifts also become systematically deshielding with increasing total layer charge, but the correlation is not as good as with $^{[4]}$Al substitution (Fig. 9, Table 6). However, as discussed below, this correlation fails for ephesite.

TABLE 4. $^{[4]}$Al/($^{[4]}$Al + $^{[6]}$Al) ratios calculated from structural formulae and from NMR spectra for 2:1 layer silicates examined in this study

Mineral	Formula	NMR (11.74 T)	NMR (6.35 T)
Black Jack beidellite	0.212	0.219	0.228
Ballarat saponite	0.906	0.98	—
Allt Ribhein saponite	0.971	1.00	—
Synthetic saponite	—	0.805	0.774
Tatatilla montmorillonite	0.060	0.067	—
Wyoming montmorillonite	0.039	0.060	—
Arizona montmorillonite	0.066	—	—
Clay Spur montmorillonite	0.096	0.095	—
Belle Fourche montmorillonite	0.060	0.066	—
Polkville montmorillonite	0.000	0.000	—
Umiat montmorillonite	0.051	0.106	—
Otay montmorillonite	0.018	0.000	—
Almeria montmorillonite	0.169	0.040	—
Interlake illite	0.270	0.293	0.320
Wind River illite	0.256	0.252	0.328
Synthetic mica-montmorillonite	0.262	0.243	0.298
Rectorite	0.260	0.261	0.276
Zemplini I/S	—	0.281	0.374
Carbago chlorite	—	0.477	—
Cookeite	0.200	0.193	0.231
Vermiculite	0.884	0.908	—
Ephesite	0.500	0.549	0.561
Palygorskite	0.140	0.104	0.128
Pyrophyllite	—	—	—
Synthetic gibbsite	—	—	—

TABLE 5. $^{[4]}$Al isotropic ^{27}Al chemical shifts and SOQE values

Mineral	δ_i* (ppm)	SOQE* (MHz)
Black Jack beidellite	72.2	2.54
Ballarat saponite	68.0	2.56
Allt Ribhein saponite	68.8	3.20
Synthetic saponite	68.6	2.90
Tatatilla montmorillonite	70.8	2.37
Wyoming montmorillonite	—	—
Arizona montmorillonite	—	—
Interlake illite	72.5	3.00
Wind River illite	71.8	2.86
Synthetic mica-montmorillonite	72.4	2.78
Rectorite	73.6	2.28
Zemplini I/S	73.0	2.94
Carbago chlorite	—	—
Cookeite	74.4	3.10
Vermiculite	72.0	3.91
Ephesite	76.8	2.82
Palygorskite	—	—

* These values were evaluated by use of the 11.74-T peak chemical shifts and the 6.35-T M1 values and the method described by Lippmaa et al. (1986). SOQE is defined as (QCC) $(1 + \eta^2/3)^{1/2}$, where QCC is the conventional nuclear electric quadrupole coupling constant and η is the asymmetry parameter of the electrostatic field gradient at the atomic nucleus.

The $^{[4]}$Al SOQE values generally increase with increasing $^{[4]}$Al substitution (Fig. 10), apparently correlating well because of AlO_4 tetrahedral shear strain (Ghose and Tsang, 1973) resulting from tetrahedral sheet distortion. These authors define the tetrahedral shear strain $|\psi|$ as the sum of the absolute values of the tangent of the difference (Δ) between the individual O–Al–O bond angles and the ideal bond angle (109.5°). The tabulated data for aluminosilicates correlates well with the relationship $|\psi| = 0.10 \cdot$ (SOQE). Use of the linear-regression correlation (Table 6) and this relationship yields $|\psi| = 0.387\ ^{[4]}\text{Al}/(^{[4]}\text{Al} + \text{Si}) + 0.222$. Use of this relationship gives $\Delta = 2.2°$ for no $^{[4]}$Al substitution and $\Delta = 3.0°$ for $^{[4]}\text{Al}/(^{[4]}\text{Al} + \text{Si}) = 0.25$. The data for ephesite, rectorite, and muscovite fall below the correlation line for other dioctahedral minerals. These phases are discussed below.

The $^{[4]}$Al SOQE values correlate better with total layer charge (Fig. 11, Table 6), and the data point for ephesite now falls along the correlation line for dioctahedral phases.

Because distortions in the tetrahedral layer correlate well with both δ_i and SOQE, there must be a correlation between δ_i and SOQE (Fig. 12). Again, the open squares representing muscovite, rectorite, and ephesite were not used in the least-squares fit (see below). The data for Mg-bearing trioctahedral minerals fall along the lower line. This correlation agrees with the superposition model (Newman and Urban, 1975) in which the quantity of interest is analyzed into individual contributions and expressed as a sum of them. The ^{27}Al δ_i and SOQE each can be expressed as a sum of contributions from the coordinated oxygen atoms. These contributions depend on the

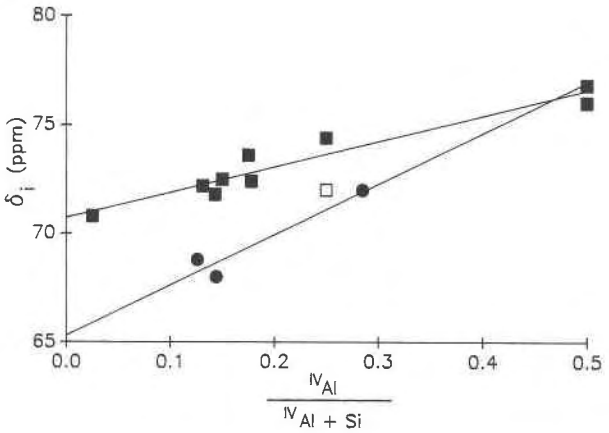

Fig. 8. ^{27}Al isotropic chemical shifts of $^{[4]}$Al vs. amount of $^{[4]}$Al substitution in layer silicates. Circle symbols represent Mg-bearing trioctahedral clays, and square symbols represent all other clays in this figure and the following figures. Lines in these figures are least-squares fit to the filled symbols.

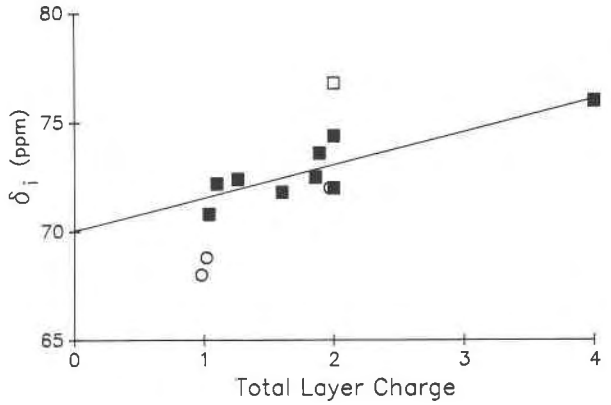

Fig. 9. ^{27}Al isotropic chemical shifts of $^{[4]}$Al vs. total layer charge in layer silicates.

structure of the polyhedron and, thus, on distortions. Such and Lehman (1988) reported reasonable agreement of this model with polyhedron distortion for the ^{25}Mg QCC and ^{29}Si chemical-shift anisotropy for forsterite and better agreement for ^{27}Al QCC for a number of minerals.

Peak shapes and atomic substitution

Second-order quadrupole MAS NMR peak shapes. The second-order quadrupole effect greatly broadens the ^{27}Al NMR peaks of most solids, and understanding these effects is essential to interpreting the data presented here. At a given H_0 magnetic field, the width of an MAS NMR peak is determined by the quadrupole coupling constant (QCC), and the shape of the peak is determined by the asymmetry parameter (η) of the electrostatic field gradient at the nucleus (Ganapathy et al., 1982; Meadows et al., 1982; Oldfield and Kirkpatrick, 1985). Figure 1 shows the 6.35-T ^{27}Al MAS NMR peaks calculated for several different values of η for QCC = 3.0 MHz. These peaks include only a nominal amount of Guassian line broadening (100 Hz) and thus contain sharp singularities. Figure 2 contains simulated peaks for the same second-order quadrupole parameters as in Figure 1 but with more Gaussian line broadening (700 Hz). These peaks are nearly symmetric, although remnants of peak structure are visible. More line broadening leads to symmetric bell-shaped peaks.

Line-broadening mechanisms. NMR interactions such as magnetic dipolar broadening, magnetic susceptibility anisotropy (VanderHart et al., 1981), and distributions of chemical shifts and QCCs can lead to peak broadening that can be approximated by Gaussian shapes. Magnetic dipolar coupling involving quadrupolar nuclei causes broadening because it does not have the familiar ($3\cos^2\theta - 1$) angular dependence and, hence, is not completely removed by rapid magic-angle spinning (Zumbulyadis et al., 1981). Also, spin relaxation causes Lorentzian nuclear-spin-energy-level lifetime broadening (Andrew, 1955).

Measurements at different H_0 fields allow assessment of the relative importance of second-order quadrupole parameters vs. line-broadening mechanisms in determining the shape and linewidth characteristics of an observed NMR peak composed of overlapping peaks from different sites. In ppm units, the contribution of isotropic chemical-shift differences and anisotropic magnetic susceptibility to shape and linewidth are independent of H_0, whereas the contribution of different quadrupole coupling constants at 6.35 T is 3.44 times that of 11.74 T. The linewidth ratios for $^{[6]}$Al in Table 3 are quite close to this value, indicating the predominance of second-order quadrupole effects in most samples. Lorentzian lifetime broadening can be significant in some samples. ^{27}Al spin-lattice relaxation times in minerals vary over several orders of magnitude and can contribute more than 100 Hz to the $^{[4]}$Al-peak linewidth of beidellite (Woessner, unpub. data).

Peak multiplicity. The ^{27}Al NMR peaks of the clay minerals do not show the sharp singularities of the simulated peaks with small line broadening, but many peaks are not symmetric either, especially those for $^{[6]}$Al. Thus, the observed peaks do not arise simply from one site with a large amount of line broadening. They can arise from several sites with the same coordination numbers but dif-

TABLE 6. Coefficients and constants for linear-regression correlations of $^{[4]}$Al δ_i and SOQE values vs. structural and compositional parameters (P)

Relationship	a	b	R
δ_i vs. $^{[4]}$Al substitution (dioct.)	11.686	70.725	0.965
δ_i vs. $^{[4]}$Al substitution (trioct.)	23.269	65.295	0.957
δ_i vs. total layer charge (dioct.)	1.521	70.024	0.861
SOQE vs. $^{[4]}$Al substitution (dioct.)	3.874	2.217	0.973
SOQE vs. total layer charge (dioct.)	0.5703	1.900	0.977
δ_i vs. SOQE (dioct.)	2.716	64.811	0.923
δ_i vs. SOQE (trioct.)	2.999	59.925	0.958

Note: Equations are of the form $\delta_i = aP + b$ (see Figs. 8, 9, 10, 11, and 12 for plots showing the points used in these correlations).

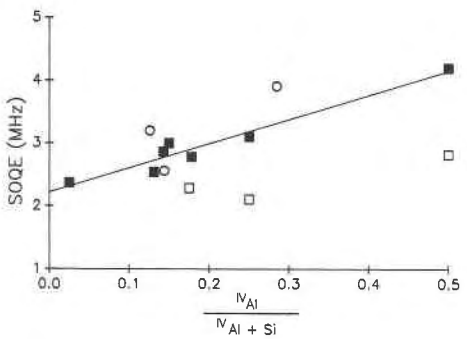

Fig. 10. ^{27}Al SOQE values of [4]Al vs. amount of [4]Al substitution in layer silicates.

ferent isotropic chemical-shift and second-order quadrupole parameters.

The asymmetry of [6]Al peaks probably arises from several sites with the same coordination and similar δ_i values, but different QCC and η values, and is most clear for the layered aluminum hydroxide gibbsite which can be considered to provide a prototype octahedral sheet for clay minerals. The 6.35-T spectrum of a very pure synthetic gibbsite obtained with a 1.8-μs 90° pulse (⅓ of a solution 90° pulse) (Fig. 3A) shows peaks at 4.3, −5.9, and −22.9 ppm and shoulders at −34 and −45 ppm. The simulated spectrum in Figure 3B indicates that the observed spectrum is consistent with two different [6]Al environments having similar δ_i values. In this simulation, one peak has 58% of the Al, δ_i = 11.0 ppm, QCC = 2.0 MHz, η = 0.8, 150-Hz Gaussian line broadening, and 150-Hz Lorentzian broadening. The other peak has 42% of the Al, δ_i = 9.0 ppm, QCC = 4.30 MHz, η = 0.40, 150-Hz Gaussian broadening, and 190-Hz Lorentzian broadening. Figure 3C shows these simulation components. A natural gibbsite sample from Minas Gerais, Brazil, yields a similar but less well resolved spectrum.

A comparison of ^{27}Al spectra from several different phases is useful in determining the causes of [6]Al-peak multiplicity. Pyrophyllite, the prototype for dioctahedral phases, is formed of sandwiches of a dioctahedral gibbsite sheet between two tetrahedral sheets that contain only Si. Its 6.35-T and 2.35-T ^{27}Al MAS NMR peaks are narrow, nearly symmetric, and appear as single sites (Fig. 4; see

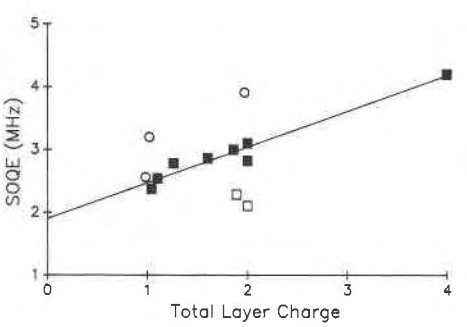

Fig. 11. ^{27}Al SOQE values of [4]Al vs. total layer charge in layer silicates.

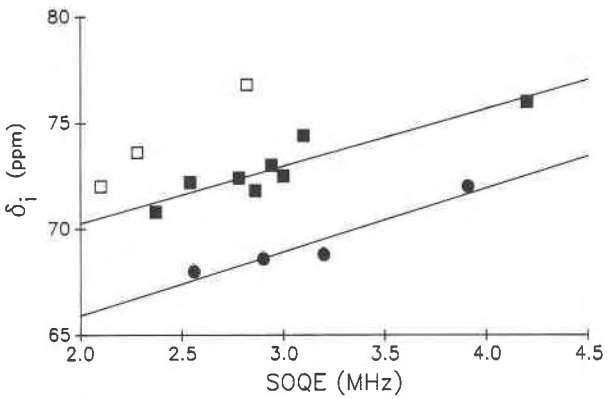

Fig. 12. ^{27}Al isotropic chemical shifts of [4]Al vs. SOQE in layer silicates.

also Kinsey et al., 1985). The shape of the 2.35-T peak is closer to that of Figure 2A than to Figure 2D, suggestive of an η value near zero. The SOQE value obtained from the 2.35-T spectrum (M1 = −13.8 ppm) and the 6.35-T M1 value (Table 2) is small, 1.4 MHz. A single QCC and η value would be expected only if the occupied and vacant octahedral sites are perfectly ordered. Although the H_0 dependences of M1 and peak shape indicate only a single small effective QCC value, multiple sites with similar, small values cannot be ruled out.

These observations for pyrophyllite aid in interpreting the [6]Al peak of gibbsite. The relatively small [6]Al QCC for pyrophyllite with no indications of multiplicity may indicate that disorder of vacant and occupied octahedral sites within an octahedral sheet is not the cause of the [6]Al site multiplicity of gibbsite (unless pyrophyllite is perfectly ordered). If this is the case, the site multiplicity for gibbsite arises from intersheet causes such as the stacking disorder. Hydroxyl groups with different orientations near the vacancy compared to near the two occupied sites, together wtih 60°, 120°, and 180° relative rotations of site vacancies in consecutive stacked sheets, could cause multiple QCC and η values at the occupied sites (R. C. Reynolds, pers. comm.).

Replacement of tetrahedral Si by Al also appears to alter the symmetry of the two [6]Al sites associated with that tetrahedral site and, thus, the QCC and η values for these sites (Barron et al., 1985). For instance, the [6]Al NMR peak of Black Jack beidellite [[4]Al/([4]Al + [6]Al) = 0.131, Fig. 5] is asymmetric and broader at its base than that of pyrophyllite at 6.35 T. This peak is qualitatively similar to that of gibbsite in that each has a narrow component of about 10 ppm linewidth and a broader component of 30–60 ppm linewidth, although singularities are not observable for the beidellite. Lippmaa et al. (1986) also reported that the [6]Al QCC of muscovite with [4]Al/(Si + [4]Al) = 0.25 is 2.2 ± 0.3 MHz and that of margarite with [4]Al/(Si + [4]Al) = 0.5 is 6.3 ± 1.0 MHz, confirming this expectation for brittle micas.

Substitution of [6]Mg for [6]Al also broadens the [6]Al MAS NMR peak by increasing the QCC of the remaining

Al. This effect appears to arise from a direct contribution to the electrostatic field gradient by the substitution of a different ionic charge and from octahedron distortions by the substitution of a different ionic radius. The 6.35-T $^{[6]}$Al peak of Tatatilla montmorillonite ($Mg/^{[6]}Al = 0.27$; Fig. 6), for instance, is much broader than that of pyrophyllite (33.1 ppm compared to 6.8 ppm). It is also broader than that of Blackjack beidellite ($Mg/^{[6]}Al = 0.005$, Fig. 6) even though beidellite has much greater $^{[4]}$Al substitution. Paramagnetic line broadening from Fe substitution appears to be relatively unimportant, because the Tatatilla sample has a much lower Fe content than Blackjack beidellite (Table 1), and montmorillonites with much greater Fe content have similar $^{[6]}$Al peak linewidths (Table 3).

$^{[4]}$Al/$^{[6]}$Al quantitation

The preponderance of excellent agreement between the $^{[4]}Al/(^{[4]}Al + ^{[6]}Al)$ ratios calculated from the 11.74-T ^{27}Al MAS NMR data and from the structural formulae based on published chemical analyses (Table 4) shows that ^{27}Al MAS NMR measurement is an excellent direct analytical technique to measure this ratio, in agreement with the conclusions of previous work (Alma et al., 1984; Barron et al., 1985; Goodman and Stucki, 1984; Kinsey et al., 1985; Kirkpatrick et al., 1986; Nadeau et al., 1985; Plee et al., 1985). The disagreement for several samples (Ballarat saponite and the Arizona, Umiat, Otay, and Almeria montmorillonites) is most likely to be due to structural formulae in Table 1 that do not represent the clay mineral examined by NMR. Published structural formulae may vary considerably in quality due to sample purification, accuracy of the chemical analysis, and method of structural-formula calculation. These problems are probably most important for the montmorillonites for which a small amount of impurity or error in analysis has a large relative effect on the $^{[4]}$Al content.

The $^{[4]}Al/^{[6]}Al$ quantitation by NMR reported here is superior to many previously published results (Barron et al., 1985; Diddams et al., 1984; Komareni et al., 1986; Lipsicas et al., 1984; Sanz and Serratosa, 1984a, 1984b; Thompson, 1984). The higher spinning speeds may be responsible. The superior results for 11.74 T vs. 6.35 T (much broader peaks) agree with this assessment.

One problem is that insufficient spinning speed leaves spectral artifacts that interfere with accurate quantitation. The nonspinning width of the central transition ($\frac{1}{2}, -\frac{1}{2}$) of a quadrupole nuclide at a given H_0 field is determined mainly by $(SOQE)^2$. Typically, this width is from 1 to 10 kHz, depending on the value of H_0 and of QCC. Rapid magic-angle spinning reduces this width by a factor of 0.28 (Behrens and Schnabel, 1982). Hence, just in order to remove overlap of the first spinning sideband with the center peak, the spinning speed must be 2.6 times the width (at infinite spinning speed) of the center peak at its base. Line-broadening mechanisms increase this minimum speed. Insufficient spinning speed causes overlapping of the center band with the first spinning sideband, overlapping of the first spinning sideband with the second spinning sideband, etc. The result can obscure the true baseline of the spectrum and also interfere with the correct phasing of the spectrum. When the sample contains both $^{[4]}$Al and $^{[6]}$Al with different SOQE values, the sidebands from one type of Al can overlap with the sidebands and the center peak of the other type. The resultant uncertainty in determining baseline level and spectrum phasing compounds the quantitation problem.

Higher-speed spinning spreads out the spinning sidebands and also lowers the intensity of a given sideband. The good quantitation of many samples at 6.35 T is due in large part to the 8.9-kHz spinning speed. This spinning speed (126 ppm) moves and attenuates the spinning sidebands sufficiently to leave only minor sideband overlap for many samples. The quantitation at slower speeds was completely inadequate for many of these samples.

When the SOQE values are different, accurate quantitation also requires the same central transition excitation for both $^{[4]}$Al and $^{[6]}$Al (Samoson and Lippmaa, 1983; Fenske et al., 1984). The pulse duration must be small compared to the rotational period of the sample spinner, and the pulse duration t_p should obey the condition $[(\pi t_p)/(2t_0)]^3 \ll 1$, where t_0 is the pulse duration for a solution 90° flip angle for the same pulse intensity. The t_p values of 1–2 μs usually give good quantitation for clays. This condition may be weakened if the SOQE values are approximately equal.

Discussion of individual phases

Beidellite

Beidellite is dioctahedral, and in the Black Jack sample, one-eighth of the tetrahedral sites is occupied by Al (Table 1). The NMR $^{[4]}Al/(^{[4]}Al + ^{[6]}Al)$ quantitation results (Table 4) are close to the chemical structure value 0.212. The NMR peaks are narrow, indicative of a pure, well-ordered sample. This narrowness of the peaks makes more visible the asymmetry of the octahedral peak (Fig. 5). Approximately 22% of this peak can be described by $\eta \simeq 0$ and QCC $\simeq$ 5.6 MHz. The narrow part of the $^{[6]}$Al peak is consistent with SOQE = 2.1 MHz.

Saponite

Ideal saponite has all three octahedral sites occupied by Mg and has appreciable $^{[4]}$Al for Si substitution. The present ^{27}Al NMR results (Table 4) show no $^{[6]}$Al in Allt Ribhein saponite and only about 2% in Ballarat saponite, in agreement with the ideal composition, but in disagreement with the structural formulae in Table 1. The spectrum of the synthetic saponite, however, shows about 20% $^{[6]}$Al with peak characteristics well suited for NMR detection (Table 4 and Fig. 6). Thus, the natural samples likely do not contain $^{[6]}$Al.

The NMR measurements indicate several differences between the natural saponites. At 6.35 T, the Allt Ribhein saponite has a significantly greater $^{[4]}$Al-peak width (20.5 ppm vs. 12.5 ppm) owing to a greater SOQE value (3.20

vs. 2.56 MHz) and a consequent greater line broadening. Since (1) the $^{[6]}$Al substitution is very low in both samples, (2) the $^{[6]}$Fe substitution is similar, and (3) the degree of $^{[4]}$Al substitution is similar (Table 1), this SOQE value difference may be due to different ordering of the $^{[4]}$Al. Indeed, the 6.35-T ^{29}Si spectrum of Allt Ribhein saponite has two peaks (50% at −95.2 ppm and 50% at −90.4 ppm), whereas that of Ballarat saponite has three peaks (70% at −95.8 ppm, 22% at −90.6 ppm, and 8% at −85.1 ppm; Woessner, unpub. data). This means that in Allt Ribhein saponite, 50% of the silicons have no next-nearest-neighbor (NNN) $^{[4]}$Al and 50% have one NNN $^{[4]}$Al. However, in Ballarat saponite, 70% of the silicons have no NNN $^{[4]}$Al, 22% one, and 8% two. These ^{29}Si NMR peak distributions for samples with similar $^{[4]}$Al/(Si + $^{[4]}$Al) ratios indicate that the two saponites have very different $^{[4]}$Al ordering that could substantially affect the ^{27}Al SOQE values.

Montmorillonite

Montmorillonite is dioctahedral but with some Mg-for-$^{[6]}$Al substitution and, for some samples, $^{[4]}$Al-for-Si substitution. This Mg-for-$^{[6]}$Al substitution results in a fourfold increase of the ^{27}Al NMR linewidth compared to beidellite at 6.35 T (Fig. 6, Table 3). To further examine this effect and to evaluate the proportion of $^{[4]}$Al vs. $^{[6]}$Al, an additional set of montmorillonite samples was examined by ^{27}Al MAS NMR at 11.74 T only (Table 3). The vast majority have similar, large $^{[6]}$Al NMR linewidths in the range 10.7 to 13.6 ppm. Variations in these widths may reflect variations in the amount and ordering of Mg substitution. However, there is no apparent correlation between Mg substitution and linewidth. Paramagnetic effects due to the substitution of Fe can also broaden the NMR line; but the broad ^{27}Al NMR line for Tatatilla montmorillonite, which has an extremely low Fe content (Table 1), indicates that Fe is not a major cause of line broadening. For example the Umiat sample has 36 times as much octahedral Fe^{3+} as Tatatilla (Table 1), but the linewidth is only slightly greater (10.7 ppm compared to 10.2 ppm, Table 7). The increased Fe content does greatly increase the spinning-sideband intensities (Fig. 7).

The ^{27}Al MAS NMR spectra of most of the montmorillonite samples show no discernible $^{[4]}$Al after the samples have been carefully purified by sedimentation. Some of the unpurified samples, however, yield a peak at 55 to 60 ppm (at 11.74 T) due to $^{[4]}$Al in framework silicates (Kirkpatrick et al., 1985a; Yang et al., 1986; Kirkpatrick et al., 1986; Lippmaa et al., 1986). The Clay Spur sample (Fig. 7) shows such $^{[4]}$Al even though the X-ray powder-diffraction analysis does not reveal framework silicate impurities. The Almeria sample (Fig. 7) does have X-ray–detectable K-feldspar. Thus, ^{27}Al NMR can readily measure $^{[4]}$Al/$^{[6]}$Al in clays and also distinguish this Al from the $^{[4]}$Al of common impurities such as feldspars and zeolites. This capability enables NMR to determine the contribution of tetrahedral Al to the clay-mineral cation-exchange capacity even when such impurities are present.

Illite

Illite is dioctahedral, but has less $^{[4]}$Al-for-Si substitution than muscovite. The Interlake illite (Fig. 6) is an excellent, rare illite with no smectite layers (R. C. Reynolds, pers. comm.), and the Wind River illite is similar. The ^{27}Al NMR data for these samples (Table 5) indicate that approximately one-fourth of the Al is $^{[4]}$Al, in excellent agreement with chemical analysis (Table 1). The $^{[6]}$Al NMR peaks are asymmetric, indicating multiple site environments due to octahedral-sheet Mg substitution and $^{[4]}$Al-for-Si substitution, but are narrower than for most montmorillonites. Also, the ratios of the $^{[6]}$Al NMR linewidths at 6.35 and 11.74 T are less than 3.44, indicating the presence of significant line-broadening mechanisms, such as magnetic susceptiblity anisotropy and relaxation lifetime broadening, in addition to the second-order quadrupolar shift.

Mixed-layer illite-smectites

The mixed-layer illite-smectite, (I/S), synthetic mica-montmorillonite (about 22% smectite layers), rectorite (ISIS ordered I/S), and Zemplini I/S (IIIS ordered I/S) yield ^{27}Al MAS NMR spectra generally similar to those from the pure illites (Figs. 6 and 7).

The $^{[4]}$Al/($^{[4]}$Al + $^{[6]}$Al) ratios of these clays are comparable to the pure illites (Table 4), and at 11.74 T the Al quantitation is excellent. However, the Zemplini I/S clay gives a large error in this ratio at 6.35 T (Table 4), due to spinning-sideband interference from the $^{[6]}$Al peak.

The correlation of SOQE of rectorite with $^{[4]}$Al substitution and total layer charge is poor (Figs. 10 and 11, open squares; $^{[4]}$Al/($^{[4]}$Al + Si) = 0.175 and total layer charge = 1.89). This observation can be rationalized as follows. Barron et al. (1985) reported that the tetrahedral illite sheets of rectorite are mica ($Si_{3.016}Al_{0.984}$) of very nearly muscovite composition (Si_3Al_1) and the tetrahedral smectite sheets are of composition ($Si_{3.587}Al_{0.414}$). Muscovite also shows poor correlation of SOQE with $^{[4]}$Al substitution and total layer charge (Figs. 10 and 11, open squares; $^{[4]}$Al/($^{[4]}$Al + Si) = 0.25 and total layer charge = 2). Although the reason for this poor correlation of muscovite is not known, this observation can be used to explain the poor correlation for rectorite. The SOQE value for this material, then, is the root-mean-square weighted average of an abnormally low muscovite value (2.1 MHz, Lippmaa et al., 1986) and a low smectite value that corresponds to that for $^{[4]}$Al/($^{[4]}$Al + Si) = 0.103 in Figure 10, resulting in a low net value.

Chlorite

Chlorites can be dioctahedral or trioctahedral, but have metal hydroxides in the interlayer space instead of large cations. Most chlorites contain a large amount of paramagnetic Fe, which obliterates the NMR signals, but spectra for two samples, Carbago chlorite and cookeite, have been obtained.

Cookeite is dioctahedral with $^{[6]}$Al and has an $^{[4]}$Al/($^{[4]}$Al

+ Si) ratio of 0.25. The hydroxide interlayer is trioctahedral with two aluminums and one Li. The δ_i ^{27}Al for $^{[4]}$Al in cookeite is 74.4 ppm, 1.9 to 3.6 ppm more deshielded than for the illites and montmorillonites. This increased deshielding is predominantly due to the increased $^{[4]}$Al substitution (filled square in Fig. 8; $^{[4]}$Al/($^{[4]}$Al + Si) = 0.25), but may be in part due to the Li in the interlayer (Weiss et al., 1987).

The $^{[6]}$Al NMR peak for cookeite is symmetric, even at 6.35 T (Fig. 6), indicating similar environments for the $^{[6]}$Al in the octahedral and hydroxide layers.

The Carbago chlorite sample has 10 to 20% sodic plagioclase impurity that is responsible for the 60.7-ppm peak in the 11.74-T spectrum (Fig. 7). A structural formula for the Carbago chlorite is not available, but the (001) X-ray powder-diffraction intensities indicate that this material is a magnesium chlorite. The 71 ppm ^{27}Al δ_i for this sample is 3–4 ppm more shielded than that of cookeite, probably owing to the trioctahedral Mg in the interlayer.

Vermiculite

Vermiculite is trioctahedral (like saponite) with some $^{[6]}$Al-for-Mg substitution, a large amount of $^{[4]}$Al-for-Si substitution, and Mg in the interlayer. The ^{27}Al NMR spectra of Llano vermiculite (Figs. 6 and 7) yield a $^{[4]}$Al/($^{[4]}$Al + $^{[6]}$Al) ratio in agreement with chemical analysis (Table 4). The large $^{[4]}$Al NMR linewidth (30.6 ppm at 6.35 T, Table 3) is the result of a relatively large SOQE value (3.91 MHz, Table 6). This large SOQE value and the ^{27}Al δ_i value, which is 3.5 ppm less shielded than that of saponite (Table 5), probably reflect the greater $^{[4]}$Al substitution (Fig. 8, filled circle; $^{[4]}$Al/($^{[4]}$Al + Si) = 0.285).

Ephesite

Ephesite, like margarite, is a brittle mica with one-half of the tetrahedral positons occupied by Al. However, unlike either muscovite or margarite, it is trioctahedral with two aluminums and one Li in the octahedral sites and Na instead of Ca in the interlayer.

The $^{[6]}$Al MAS NMR peak of ephesite is broad and shows structure (Fig. 6) that can be simulated with the parameters δ_i = 10.4 ppm, QCC = 5.7 MHz, and η = 0.3. These parameters are similar to those reported for margarite (δ_i = 11 ± 4 ppm, QCC = 6.3 ± 1.0 MHz, and η = 0.1 ± 0.1; Lippmaa et al., 1986). This similarity shows that the filling of the octahedral vacancies by the Li has only a minor affect on the $^{[6]}$Al NMR parameters.

The failure of the $^{[4]}$Al chemical shift of ephesite to fall along the correlation line for trioctahedral phases (Fig. 9) can be rationalized by noting that an octahedral site occupied by Li is the same size as the vacancy (Bailey, 1980). Thus, it should not affect the tetrahedral sheet distortion, and, thus, the $^{[4]}$Al chemical shift should fall along the correlation line for dioctahedral minerals as observed [Fig. 8, upper filled square; $^{[4]}$Al/($^{[4]}$Al + Si) = 0.5]. The $^{[4]}$Al δ_i for ephesite does not fall along the correlation of dioctahedral phases with total layer charge (open square, Fig. 9). If the layer charge is doubled (to counteract the charge due to the Li substitution), however, this point falls on the correlation. Therefore, the effect of total layer charge on δ_i is due to lattice distortion, and the Li charge substitution (which does not distort the lattice) has little effect on δ_i. The ^{29}Si MAS NMR spectrum supports these conclusions. The ^{29}Si δ_i for ephesite is −75.9 ppm, whereas that for margarite is −75.5 ppm, indicating similar tetrahedral distortions (Woessner, unpub. data).

The $^{[4]}$Al SOQE value of ephesite correlates well with total layer charge (Fig. 11, lower filled square; total layer charge = 2) but poorly with $^{[4]}$Al substitution [open square at $^{[4]}$Al/($^{[4]}$Al + Si) = 0.5, Fig. 10]. The data for margarite correlate well with both. Thus, the change in charge distribution resulting from octahedral Li substitution counteracts part of the SOQE value resulting from tetrahedral sheet distortion.

The value of 55% for $^{[4]}$Al/($^{[4]}$Al + $^{[6]}$Al) determined by NMR is close to the value for "ideal" ephesite.

Palygorskite

Palygorskite (formerly called attapulgite) is composed of 2:1 ribbons that are linked to each other laterally by single basal oxygens. There are five cation positions across the octahedral strip, but all are not necessarily occupied. There is little $^{[4]}$Al. In the sample examined, 1.96 octahedral sites are filled by Mg and 1.29 by Al. The $^{[6]}$Al MAS NMR peak is unusual, because it is symmetric and at nearly the same ppm value at all three H_0 field strengths. Thus, the SOQE value is small (0.9 MHz), and δ_i, = 5.5 ppm. The SOQE value is the smallest known for clay minerals, indicating that the AlO_6 tetrahedra are very regular. The peaks have relatively long tails, similar in shape to Figure 2D, indicating an η value near 1.

Conclusions

Magic-angle-spinning ^{27}Al NMR at high H_0 magnetic field strengths provides a means of characterizing 2:1 clay minerals on the basis of the local chemical and structural environment of the Al atoms. The isotropic chemical shifts and nuclear electric quadrupole coupling values increase with the tetrahedral lattice distortion arising from increasing $^{[4]}$Al substitution and total layer charge. This correlation agrees with the findings of Such and Lehman (1988) that QCC and anisotropy of the chemical shift are determined largely by the distortion of the first coordination sphere of the central ion. The quadrupole coupling can also be affected by a direct electrostatic interaction with ionic charges (Villa and Bjorkstam, 1983).

The chemical-shift difference between $^{[4]}$Al in clays and framework silicate impurities such as feldspars, glasses, and zeolites enables determination of clay $^{[4]}$Al/$^{[6]}$Al even when such contaminants are present. Excellent quantitation of $^{[4]}$Al/$^{[6]}$Al is possible under the above conditions. This ability can be important for the calculation of clay structural formulae, especially when used in conjunction with absolute Al quantitation (Kirkpatrick et al., 1986). Chemical analysis gives the total, overall elemental com-

position of the sample. The usual method of structural-formula calculation of a 2:1 layer involves assigning all of the Si to the tetrahedral layer and then apportioning enough Al to bring the total tetrahedral cations to 8. Since the number of silicons in a montmorillonite is typically 7.5–8, contaminants can readily cause error in this method. Even when no contaminant is present, a 1% error in Si analysis would result in a minimum 15% relative error in the $^{[4]}$Al content. NMR has a distinct advantage for such determinations. In particular, it is a direct and sensitive technique (Nadeau et al, 1985) compared to the otherwise complex procedures for distinguishing montmorillonite from beidellite (Malla and Douglas, 1987) and for determining the tetrahedral-layer charge (Nadeau and Bain, 1986).

The broad asymmetric $^{[6]}$Al NMR peak of many 2:1 clay minerals indicates multiple octahedral-site environments that differ mainly in SOQE value. The site differences are sensitive to $^{[4]}$Al substitution and especially to octahedral-sheet Mg substitution. Multiple-H_0-strength ^{27}Al MAS NMR measurements with ultra–high speed spinning should be useful in studies of $^{[6]}$Al-site environments. The effects of Mg substitution are complicated, as shown by the lack of correlation between $^{[6]}$Al NMR peak linewidth and amount of Mg substitution. The peak linewidth may be a complicated function of the amount of Mg substitution and the ordering of the site substitutions. Since the peaks from the various $^{[6]}$Al-site environments may not be resolved, the use of M1 values may be informative.

Acknowledgments

I acknowledge W. S. Callaway, J. T. Edwards, J. B. Higgins, R. C. Reynolds, and S. E. Sommer for samples and information on clay mineralogy. J. T. Edwards characterized the samples by X-ray powder diffraction. I am especially thankful for the stimulating discussions with L. B. Alemany, J. G. Bendoraitis, L. Green, and J. C. Trewella at the Riverside Conference Center concerning the ubiquity of albite. The suggestions of R. J. Kirkpatrick, J. T. Edwards, and R. C. Reynolds resulted in a significant improvement of the original manuscript.

References cited

Alma, N.C.M., Hays, G.R., Samoson, A.V., and Lippmaa, E.T. (1984) Characterization of synthetic dioctahedral clays by solid-state silicon-29 and aluminum-27 nuclear magnetic resonance spectrometry. Analytical Chemistry, 56, 729–733.

Anderson, D.M., and Reynolds, R.C. (1966) Umiat bentonite: An unusual montmorillonite from Umiat, Alaska. American Mineralogist, 51, 1443–1456.

Andrew, E.R. (1955) Nuclear magnetic resonance, 120 p. University Press, Cambridge.

Bailey, S.W. (1980) Structures of layer silicates. In G.W. Brindley and G. Brown, Eds., Crystal structures of clay minerals and their X-ray identification, p. 1–123. Mineralogical Society, London.

Barron, P.F., Slade, P., and Frost, R.L. (1985) Ordering of aluminum in tetrahedral sites in mixed-layer 2:1 phyllosilicates by solid-state high-resolution NMR. Journal of Physical Chemistry, 89, 3880–3885.

Behrens, H.-J., and Schnabel, B. (1982) The second-order influence of the nuclear quadrupole interaction on the central line in the NMR of quadrupolar nulcei using rapid sample spinning. Physica, 114B, 185–190.

Bradley, W.F. (1940) The structural scheme of attapulgite. American Mineralogist, 25, 405–410.

Callaway, W.S., III, and McAtee, J.L., Jr. (1985) Magnetic susceptibilities of representative smectites. American Mineralogist, 70, 996–1003.

Diddams, P.A., Thomas, J.M., Jones, W., Ballentine, J.A., and Purnell, J.H. (1984) Synthesis, characterization, and catalytic activity of beidellite-montmorillonite layered silicates and their pillared analogues. Journal of the Chemical Society, Chemical Communications, 1340–1342.

Fenske, D., Freude, D., Frohlich, T., and Haase, J. (1984) NMR intensity measurements of half-integer quadrupole nuclei. Chemical Physics Letters, 111, 171–175.

Ganapathy, S., Schramm, S., and Oldfield, E. (1982) Variable-angle sample-spinning high-resolution NMR of solids. Journal of Chemical Physics, 77, 4360–4365.

Ghose, S., and Tsang, T. (1973) Structural dependence of quadrupole coupling constant e^2qQ/h for ^{27}Al and crystal field parameter D for Fe^{3+} in aluminosilicates. American Mineralogist, 58, 748–755.

Goodman, B.A., and Stucki, J.W. (1984) The use of nuclear magnetic resonance (NMR) for the determination of tetrahedral aluminum in montmorillonite. Clay Minerals, 19, 663–667.

Hafner, S., and Hartmann, P. (1964) Electrische feldgradienten und sauerstoff-polarisierbarkeit in alkali-feldspaten ($NaAlSi_3O_8$ und $KalSi_3O_8$). Helvetica Physica Acta, 37, 348–360.

Hower, J., and Mowatt, T.C. (1966) The mineralogy of illites and mixed layer illite/montmorillonites. American Mineralogist, 51, 825–854.

Kinsey, R.A., Kirkpatrick, R.J., Hower, J., Smith, K.A., and Oldfield, E. (1985) High resolution aluminum-27 and silicon-29 nuclear magnetic resonance spectroscopic study of layer silicates, including clay minerals. American Mineralogist, 70, 537–548.

Kirkpatrick, R.J., Kinsey, R.A., Smith, K.A., Henderson, D.M., and Oldfield, E. (1985a) High resolution solid-state sodium-23, aluminum-27, and silicon-29 nuclear magnetic resonance spectroscopic reconnaissance of alkali and plagioclase feldspars. American Mineralogist, 70, 106–123.

Kirkpatrick, R.J., Smith, K.A., Schramm, S., Turner, G., and Yang, W.-H. (1985b) Solid-state nuclear magnetic resonance spectroscopy of minerals. Annual Reviews of Earth and Planetary Sciences, 13, 29–47.

Kirkpatrick, R.J., Oestrike, R., Weiss, C.A., Jr., Smith, K.A., and Oldfield, E. (1986) High-resolution ^{27}Al and ^{29}Si NMR spectroscopy of glasses and crystals along the join $CaMgSi_2O_6$-$CaAl_2SiO_6$. American Mineralogist, 71, 705–711.

Komareni, S., Fyfe, C.A., Kennedy, G.J., and Strobl, H. (1986) Characterization of synthetic and naturally occurring clays by ^{27}Al and ^{29}Si magic-angle spinning NMR spectroscopy. Journal of the American Ceramic Society, 69, C-45–C-47.

Lippmaa, E., Samoson, A., and Magi, M. (1986) High-resolution ^{27}Al NMR of aluminosilicates. Journal of the American Chemical Society, 108, 1730–1735.

Lipsicas, M., Raythatha, R.H., Pinnavaia, T.J., Johnson, I.D., Giese Jr., R.F., Costanzo, P.M., and Robert, J.-L. (1984) Silicon and aluminum site distributions in 2:1 layered silicate clays. Nature, 309, 604–607.

Mackenzie, R.C. (1957) Saponite from Allt Ribhein, Fiskavaig Bay, Skye. Mineralogical Magazine, 31, 672–680.

——— (1960) The evaluation of clay mineral composition with particular reference to smectites. Silicates Industry, 25, 12–18, 71–75.

Malla, P.B., and Douglas, L.A. (1987) Problems in identification of montmorillonite and beidellite. Clays and Clay Minerals, 35, 232–236.

Meadows, M.D., Smith, K.A., Kinsey, R.A., Rothgeb, T.M., Skarjune, R.P., and Oldfield, E. (1982) High-resolution solid-state NMR of quadrupolar nuclei. Proceedings of the National Academy of Sciences, 79, 1351–1355.

Nadeau, P.H., and Bain, D.C. (1986) Composition of some smectites and diagenetic illitic clays and implications for their origin. Clays and Clay Minerals, 34, 455–464.

Nadeau, P.H., Farmer, V.C., McHardy, W.J., and Bain, D.C. (1985) Compositional variations of the Unterrupsroth beidellite. American Mineralogist, 70, 1004–1010.

Newman, D.J., and Urban, W. (1975) Interpretation of S-state ion E.P.R. spectra. Advances in Physics, 24, 793–844.

Oldfield, E., and Kirkpatrick, R.J. (1985) High-resolution nuclear magnetic resonance of inorganic solids. Science, 227, 1537–1544.

Plee, D., Borg, F., Gatineau, L., and Fripiat, J.J. (1985) High resolution solid-state ^{27}Al and ^{29}Si nuclear magnetic resonance study of pillared clays. Journal of the American Chemical Society, 107, 2362–2369.

Samoson, A., and Lippmaa, E. (1983) Excitation phenomena and line intensities in high-resolution NMR powder spectra of half-integer quadrupolar nuclei. Physical Review B, 28, 6567–6570.

Sanz, J., and Serratosa, J.M. (1984a) Distinction of tetrahedrally and octahedrally coordinated Al in phyllosilicates by NMR spectroscopy. Clay Minerals, 19, 113–115.

——— (1984b) ^{29}Si and ^{27}Al high-resolution MAS-NMR spectra of phyllosilicates. Journal of the American Chemical Society, 106, 4790–4793.

Schaller, W.T., Maxwell, K.C., and Fleischer, M. (1967) Ephesite, $Na(LiAl_2)(Al_2Si_2)O_{10}(OH)_2$, a trioctahedral member of the margarite group, and related brittle micas. American Mineralogist, 52, 1689–1696.

Schultz, L.G. (1969) Lithium and potassium absorption, dehydroxylation temperature, and structural water content of aluminous smectites. Clays and Clay Minerals, 17, 115–149.

Shirozu, H., and Bailey, S.W. (1966) Crystal structure of a two-layer Mg-vermiculite. American Mineralogist, 51, 1124–1143.

Shulepov, Yu.V., Litovchenko, A.S., Melnikov, A.A., Proshko, V. Ya., and Kulik, V.V. (1983) The effects of quadrupole splitting of the central ^{27}Al NMR line in polycrystalline kaolinite. Journal of Magnetic Resonance, 53, 178–186.

Such, K.P., and Lehman, G. (1988) Superposition analysis of ^{29}Si and ^{25}Mg NMR data for forsterite Mg_2SiO_4. Chemical Physics Letters, 143, 463–466.

Thompson, J.G. (1984) ^{29}Si and ^{27}Al nuclear magnetic resonance spectroscopy of 2:1 clay minerals. Clay Minerals, 19, 229–236.

VanderHart, D.L., Earl, W.L., and Garroway, A.N. (1981) Resolution in ^{13}C NMR of organic solids using high-power proton decoupling and magic-angle sample spinning. Journal of Magnetic Resonance, 44, 361–401.

Van Olphen, H., and Fripiat, J.J. (1979) Data handbook for clay minerals and other non-metallic minerals. Pergamon Press, Oxford.

Villa, Marco, and Bjorkstam, J.L. (1983) Structure and ^{27}Al NMR spectra in β-aluminas. Journal of Magnetic Resonance, 51, 349–360.

Weiss, C.A., Jr., Altaner, S.P., and Kirkpatrick, R.J. (1987) High-resolution ^{29}Si NMR spectroscopy of 2:1 layer silicates: Correlations among chemical shift, structural distortions, and chemical variations. American Mineralogist, 72, 935–942.

Yang, W.-H., Kirkpatrick, R.J., and Henderson, D.M. (1986) High-resolution ^{29}Si, ^{27}Al, and ^{23}Na NMR spectroscopic study of Al-Si disordering in annealed albite and oligoclase. American Mineralogist, 71, 712–726.

Zumbulyadis, N., Henrichs, P.M., and Young, R.H. (1981) Quadrupole effects in the magic-angle-spinning spectra of spin-½ nuclei. Journal of Chemical Physics, 75, 1603–1611.

Manuscript received October 9, 1987
Manuscript accepted October 7, 1988